

# PCCP

Accepted Manuscript



This is an *Accepted Manuscript*, which has been through the Royal Society of Chemistry peer review process and has been accepted for publication.

*Accepted Manuscripts* are published online shortly after acceptance, before technical editing, formatting and proof reading. Using this free service, authors can make their results available to the community, in citable form, before we publish the edited article. We will replace this *Accepted Manuscript* with the edited and formatted *Advance Article* as soon as it is available.

You can find more information about *Accepted Manuscripts* in the [Information for Authors](#).

Please note that technical editing may introduce minor changes to the text and/or graphics, which may alter content. The journal's standard [Terms & Conditions](#) and the [Ethical guidelines](#) still apply. In no event shall the Royal Society of Chemistry be held responsible for any errors or omissions in this *Accepted Manuscript* or any consequences arising from the use of any information it contains.

## Effect of grain boundaries on the mechanical properties and failure behavior of hexagonal boron nitride sheets

Ning Ding<sup>a,b</sup>, Chi-Man Lawrence Wu<sup>\*a,b</sup>, Hui Li<sup>\*c</sup>

<sup>a</sup> Department of Physics and Materials Science, City University of Hong Kong, Hong Kong SAR, PR China. E-mail: lawrence.wu@cityu.edu.hk (C.-M.L. Wu)

<sup>b</sup> Shandong Academy of Sciences, Jinan, PR China

<sup>c</sup> Key Laboratory for Liquid-Solid Structural Evolution and Processing of Materials, Ministry of Education, Shandong University, Jinan 250061, PR China. E-mail: lihuilmy@hotmail.com (H. Li)

**Keywords:** hexagonal boron nitride sheet, grain boundary, mechanical property, intrinsic strength

### Abstract

In this work, the effect of grain boundaries (GBs) on the mechanical properties and failure behavior of two-dimensional hexagonal boron nitride (*h*-BN) sheet are systematically and comprehensively investigated by density functional theory. Results show that the arrangement of homoelemental bonds on GBs is an important factor which could affect the atomic structures and stability of the *h*-BN sheet. The relationship between the formation energy and the misorientation angles is downward opening parabolic. The intrinsic strength shows obvious decreasing trend with increasing inflection angles, while it shows periodic dependence on the increase in misorientation angles. Thus, the mechanical properties of *h*-BN are significantly influenced by GBs. The *h*-BN sheets with different types of GBs show varied failure behavior which are caused by the distinct stress distribution on GBs. The information obtained in this study would be useful for the understanding of GBs on *h*-BN surface.

## 1. Introduction

The effect from the grain boundary (GB) is an important factor that affects the electronic, mechanical and thermal properties of materials.<sup>1</sup> The influences of GBs on the properties of various low-dimensional materials have recently been intensively investigated.<sup>2-8</sup> Significant effects of GBs on the electronic structures, magnetic properties and mechanics of graphene have been reported.<sup>9-13</sup> As a close analog of graphene, two-dimensional (2D) hexagonal boron nitride (*h*-BN) sheet is consisted of equal boron and nitrogen atoms through sp<sup>2</sup> hybridization in hexagonal rings. The 2D *h*-BN possesses many unique properties compared to graphene.<sup>14-17</sup> The chemical and thermal properties of *h*-BN are more stable than that of graphene at high temperatures and in an oxidative atmosphere.<sup>18-20</sup> The *h*-BN sheet may be an alternative to graphene when exposed to extreme conditions.

The potential industrial application of *h*-BN should be based on its potential for large-scale production. Chemical vapor deposition (CVD) is one of the most suitable methods to realize the massive production of *h*-BN sheets. In the CVD process, GBs were formed on the polycrystalline substrates where two grains meet by propagating growth fronts.<sup>15</sup> The study of GB properties is necessary to explore and evaluate the influence of these interfaces on the mechanical, thermal and electronic properties of *h*-BN sheet. As topological line defects, GBs on *h*-BN surface possess complex structures. Prior studies have shown that GBs on *h*-BN surface may be composed of pentagon-heptagon (5|7) pairs or square-octagon (4|8) pairs.<sup>21-23</sup> In 2013, Zettl *et al.* clearly observed GBs on an *h*-BN surface produced via CVD method using super-high resolution transition electronic microscopy.<sup>23</sup> They found that pentagon-heptagon (5|7) pairs were the main components of GBs on the *h*-BN surface. Defects at GBs and the dynamic behavior of GBs were also recorded. More recently in 2014, GBs with the form of (4|8) pairs were firstly discovered by Cretu *et al.* on *h*-BN surface at high sample temperature (~1000 K) under electron beam irradiation.<sup>24</sup> According to their findings, gliding of one or two atomic rows along the armchair direction is the origin of the

defect motion. Synchronously, several theoretical studies have been performed to predict the structures and electronic properties of some symmetric and asymmetric GBs on *h*-BN surface.<sup>21,22</sup> It has been pointed out that controlling GBs on *h*-BN surface may help in tuning the electronic structures and magnetic properties of the *h*-BN sheet, thus realizing the various applications of GBs in electronic and optical devices.

However, to our best knowledge, although the influence of GBs on the electronic structure and magnetic properties of *h*-BN has been investigated using theoretical methods,<sup>25-27</sup> the effect of GBs on the mechanics of *h*-BN has not been reported. According to a recent study on graphene GBs,<sup>3</sup> the effect of GBs on the mechanical properties of graphene was dependent on not only the defect density but also the distribution of GB dislocations. Although the atomic structure of 2D *h*-BN is similar to that of graphene, the two materials have essential difference attributed to the heteroelemental nature of BN. For the same (5|7) pair of GB configuration, the growth fronts of grains may form elemental polar GBs (B-rich or N-rich) or nonpolar GBs (B:N=1:1). The effect of GBs on the mechanical properties and failure behavior of *h*-BN is more complex than that of graphene, and requires further systematic investigation. Two issues should be considered: (1) the possible relationship between the mechanical properties of *h*-BN and GB parameters; and (2) the extent of effect of GB interfaces on the mechanical properties of *h*-BN.

In this work, the effects of GBs on the mechanical properties and failure behavior of *h*-BN were investigated using density functional theory (DFT). Fifteen representative *h*-BN GBs, which range from a low defect concentration to a relatively high defect concentration, were used to illustrate the influence of GB interface. This study is designed to obtain information on the relationship of the mechanics of *h*-BN and the different GB parameters.

## 2. Results and discussion

### 2.1. Nomenclature and GB models

The nomenclature of the GB model is shown in Figure 1. Typically, a GB of *h*-BN sheet can be described by two periodic translation vectors for the left domain ( $n_L, m_L$ ) and for the right domain ( $n_R, m_R$ ) of the GB along the defect direction as  $(n_L, m_L)|(n_R, m_R)$ .<sup>28</sup> The misorientation and inflection angles are defined to describe the mismatching degree between the two domains and the flexion degree of *h*-BN sheet with GBs. The orientation of a grain on the *h*-BN surface is related to not only its geometry configuration but also the arrangement of boron and nitrogen (B and N) atoms.

Fifteen types of GBs and a pristine *h*-BN surface, for reference, were explored (Figure 2). The parameters of all the GB models, including the inflection angles, misorientation angles and periodic lengths, are shown in Table 1. Most of these GBs composed of (5|7) pairs, which were observed in previous experiments<sup>23</sup> as one of the main unit cells in GBs on *h*-BN surface. In addition, we also considered two types of GBs (*i.e.*, (1,0)|(0,1) and (1,1)|(1,1)) which were formed by the homoelemental bonds (B-B or N-N bonds) and predicted by Liu *et al.* in their recent theoretical study.<sup>21</sup> To provide a clearer description of the GBs, we categorized all 15 GBs into three classes: (i) GBs with symmetric structures (sym-GB), in which the grains have mirror symmetry about the GB; (ii) GBs with asymmetric structures (asym-GB), in which the grains on one side of the GB were given an inversion relative to the sym-GB; and (iii) nonsymmetric GBs (nsym-GB).

The appearance of homoelemental bonds (B-B or N-N bonds) along GBs is an important feature for the GBs on *h*-BN surface. Usually, the two types of homoelemental bonds appeared alternately along the GB line. However, in some particular cases, unequal numbers of B-B bonds and N-N bonds along a GB line cause elemental polarity (B-rich or N-rich). A B-rich (N-rich) GB line would cause its neighboring GB line to be N-rich (B-rich) to balance the B and N atoms and ensure a 1:1 ratio. Figure 2 shows that sym-GBs and two types of nsym-GBs contain B-rich and N-rich GBs, whereas asym-GB structures do not possess

element polarity. In addition, different arrangements of the homoelemental bonds may change grain orientations. Although the arrangements of (5|7) pairs along the GB line on the GB (4,2)|(3,3)-1 and (4,2)|(3,3)-2 models are the same, their misorientation angles show a difference of  $60^\circ$  attributed to the different arrangements of the homoelemental bonds (Figure 2). In addition, (4,2)|(3,3)-1 contains B-rich and N-rich GBs, whereas (4,2)|(3,3)-2 does not show element polarity. In our calculation, the length of the calculated B-B bond of the models ranges from 1.433 Å to 1.487 Å, while that for an N-N bond ranges from 1.632 Å to 1.769 Å, which are consistent with previous research.<sup>21,22</sup>

## 2.2 Formation energy

Formation energy was used to describe the stability of GBs on *h*-BN surface, which can be calculated as<sup>29</sup>

$$E_f = (E_{tot} - E_{BN} - \sum_i n_i \mu_i) / 2L \quad (1)$$

where  $E_{total}$  and  $E_{BN}$  are the energies of the *h*-BN sheet with and without GBs, respectively.  $\mu_i$  is the increased ( $n_i > 0$ ) or decreased ( $n_i < 0$ ) chemical potential of boron (nitrogen) atoms. Formation energies of all GBs are shown in Table 1. Values of the formation energies for all the GBs range from 3.5 eV to 9.1 eV.

It is mentioned in the previous works that the formation energy of a GB originated from two aspects: the mismatch energy and the defect energy. Besides these two above aspects, energy change induced by the formation of homoelemental bonds is another factor which may affect the stability of GBs on *h*-BN surface. For example, the formation energy of GB (1,1)|(1,1) and (1,0)|(0,1), which just contain homoelemental bonds along the GB line, were 8.5 eV/nm and 7.5 eV/nm, respectively. These values are even higher than some GBs with high (5|7) pair concentration (Table 1). On the other hand, the formation energies of GBs with the same (5|7) pair arrangement but different quantity and composition of homoelemental bonds were

significantly different. For example, the difference in formation energies between (4,2)|(3,3)-1 and (4,2)|(3,3)-2 is 5.4 eV/nm, and the difference between (4,2)|(2,4) and (4,2)|(4,2) is 2.6 eV.

Figure 3 shows formation energies of the 15 GBs as functions of either the inflection angle or misorientation angle. The relationship between formation energies of GBs and the inflection angles is not very clear. However, it can be found that GBs with an inflection angle near  $30^\circ$  are lower than those of GBs with inflection angles far from  $30^\circ$ . Most *h*-BN surfaces with GBs exhibit a three-dimensional (3D) warping along the GB line (i.e., the inflection angle  $\alpha \neq 0$ ), which were also observed in previous experiments.<sup>23</sup> This behavior of GBs leads to energy release and greater stability with relatively lower formation energy respect to the flat GBs. However, when the inflection angle is larger than a particular value (here it is about  $30^\circ$ ), the energy release due to the flection of *h*-BN surface could hardly compensate the energy requirement due to the torsion of the (5|7) pairs, the formation energy will increase.

For the relationship between formation energy and misorientation angles (Figure 3(b)), the formation energies initially increase with increasing mismatch degree between the grain orientations in the two domains of GB. When the misorientation angles increase to larger than about  $60^\circ$  (which is a half angle period of a hexagonal ring on *h*-BN surface), the trend of formation energies change to decrease with the increasing of the misorientation angles. As the GB structures with different misorientation angles can be transformed into each other by planar rotations,<sup>21</sup> when the misorientation angles of a GB structure is larger than  $60^\circ$ , this structure would come close to its original structure with a misorientation angle of  $0^\circ$  ( $120^\circ$ ) due to the angle period of a hexagonal ring on *h*-BN surface. Thus, it is believed that the decrease of formation energies along the parabola ( $\theta > 60^\circ$ ) in Figure 3(b) is mainly caused by the decrease of the mismatch energy. Basically, the formation energy is sensitive to the change of the geometry of *h*-BN (with GB) surface, that is the deviation of the geometry from the pristine *h*-BN. Also, the effect of homoelemental bonds on the formation energy could not

be ignored. In our work, the formation energy is an average of B-rich and N-rich grain boundaries. If at a local area where just B-rich (or N-rich) were considered, a little deviation of the formation energy may occur. This phenomenon is caused by the different chemical potential of B and N atoms and also been stated in some other references.<sup>21</sup>

### 2.3 Intrinsic strengths

To compare the influence of GBs on the mechanical properties of *h*-BN, a series of nonaxial tensile test along the tangential direction of the *h*-BN surface and perpendicular to the GB line were performed. Stress-strain curves of *h*-BN with GBs were plotted based on the relationship between strain energy and stress. In our calculation, single-layer *h*-BN was regarded as a layer with a thickness of 0.33 nm.<sup>6</sup> Intrinsic strength, which was defined as the highest stress point along the stress-strain curve, was obtained to evaluate the mechanical performance of *h*-BN. As a reference, pristine *h*-BN was tested along its armchair and zigzag directions. The intrinsic strengths of *h*-BN is 102 GPa and 87 GPa for the zigzag and armchair directions, respectively. This result is in good agreement with the results obtained by Wei in 2013, who focused on the mechanics of pristine *h*-BN along different directions.<sup>30</sup> As shown in Figure 4, the stress-strain curves for all 15 GBs show obvious brittle fracture characteristic, i.e., rupture occurs without any prior noticeable change in the rate of elongation. The critical failure strain ranges from 11% to 21%.

As shown in Figure 5(a), intrinsic strength shows a significant decrease with the increase in the inflection angles. Generally speaking, flat GBs, such as sym-(1,0)|(0,1) and asym-(1,1)|(1,1), show the highest intrinsic strength among all the GB systems. The intrinsic strengths are 85 GPa for asym-(1,1)|(1,1) and 78 GPa for sym-(1,0)|(0,1), respectively, which are almost comparable to that of perfect *h*-BN (103 GPa or 88 GPa). As these two GBs are composed of homoelemental bonds rather than (5|7) pairs, which do not break the flat plane of the *h*-BN sheet, they provide slight influence on the GB strength (less than about 20%). When

the inflection angle of the GB reaches more than 40°, GB strength significantly decreases to less than 50% of that of the pristine *h*-BN.

The fitted line in Figure 5(a) shows that the relationship between intrinsic strength and inflection angles can be expressed as

$$\tau = \tau_0 - 0.89\alpha \quad (2)$$

where  $\tau_0 = 88$  GPa is the approximate intrinsic strength of the pristine *h*-BN. Thus, the flection of GBs significantly decreases the mechanical strength of an *h*-BN sheet. Here, lager inflection angles result in more bulking of the h-BN sheet and closer resemblance to its 3D structures. Local sp<sup>3</sup> hybridization appears in the bulk GB structures, which may reduce the intrinsic strength of this material. A similar relationship was also obtained on graphene surface.<sup>6,31,32</sup>

Intrinsic strength basically shows periodic dependence on increasing misorientation angles (Figure 5(b)). Pristine *h*-BN along the zigzag direction (with a misorientation angle of 0°) shows the highest intrinsic strength. Then the intrinsic strength of GBs decreases with the increasing mismatching degree of the two domains. When the misorientation angles increase to larger than about 30°, the intrinsic strength of GBs begin to rise. Additionally, intrinsic strength reaches another maximum when the misorientation angle approaches 60°. It is related to the GB (1,1)|(1,1), which does not contain (5|7) pairs. And then the intrinsic strength changes follow another variation circle. As mentioned above, this periodic variation law may be caused by the periodic change of the mismatch between the two domains of GBs.

Among all the 15 GBs, GB (2,4)|(5,0) shows the lowest intrinsic strength of 34GPa. As shown in Figure 2, this GB structure is constituted by separated pentagon and heptagon rings, which introduce larger tension than the (5|7) pair, thus significantly reduce the strength of the material. A similar dramatic reduction in strength caused by the separate pentagon and heptagon rings was also found on a graphene surface by Zhao and Lu.<sup>6</sup>

The intrinsic strength shows no clear correlation with the line density/concentration of GB unit, but exhibits interesting dependence on the geometry parameters of GBs. This phenomenon was also observed on graphene surface.<sup>6,7</sup> Here, to confirm the effect of GB geometries on the intrinsic strength of *h*-BN, the bond and angle distributions of three types of *h*-BN surfaces (i.e., a pristine *h*-BN, GBs (2,4)|(5,1) and (1,5)|(4,3)) were obtained and are shown in Figure 6. The distributions of bond length and bond angle for *h*-BN with GBs are significantly wider than those of pristine *h*-BN. This indicates that the atomic structure of GBs clearly deviates from the pristine *h*-BN structure, which may introduce additional stress on the surface. More importantly, GB (2,4)|(5,1) (with an intrinsic strength of 70 GPa) shows narrower distribution of bond length and bond angle, which causes its atomic structure to deviate less from the pristine *h*-BN than GB (1,5)|(4,3) (with an intrinsic strength of 56 GPa), and possess a relatively high intrinsic strength.

## 2.4 Failure Behavior

To reveal the failure behavior of GBs, the configuration of GBs with different strains were collected. Figure 7 shows the fracture process of three types of GB units. Figure 7(a) is an isolated B-rich (5|7) pair enclosed by hexagonal rings. The fracture begins with a 7-6 N-B bond (shared by a heptagon and a hexagon) rather than a B-B bond. The initial length of this bond is 1.517 Å. After breaking the 7-6 N-B bond, a meta-B-N bond in the same hexagonal ring is elongated and broken. Then, the fracture is transferred to the regular hexagonal rings along the GB line and complete failure occurs rapidly. For the isolated (5|7) pair, breaking of a 7-6 N-B bond was usually the initial sign of failure. However, in our calculation the 7-6 N-B bond both in the B-rich (5|7) pairs and N-rich (5|7) pairs is found to be possible initial breaking bond. For some particular cases, such as for GB (4,2)|(2,4), the fracture synchronously starts from two neighboring GB lines. The different initial fracture mode is

believed to be related to the stress field which are controlled by the defect distribution along the GBs.

For GB lines with consecutive (5|7) pairs (Fig. 7(b)), breaking of a 7-7 N-B bond has been found to be the first step of failure. This bond is located at the connecting point of two heptagons, which belong to two different (5|7) pairs. Then, the fracture front extends into the two neighboring (5|7) pairs along the GB line and toward opposite fracture directions (up and down). The transfer step occurs by the elongation and breaking of a 7-7 and a 7-5 N-B bonds, respectively. After the breaking of these particular bonds, the *h*-BN sheet fails rapidly along the GB line. As a GB without (5|7) pairs, the fracture process of GB (1,1)|(1,1) is different from that of the (5|7) pair GB lines (Figure 7(c)). During tensile loading, B-B and N-N bonds at the GB line are uniformly elongated, which give rise to a synchronously abrupt rupture along the GB line. This fracture characteristic is also observed on GB (1,0)|(0,1), another GB without (5|7) pairs.

### 3. Conclusions

The effect of GBs on the mechanical properties and failure behavior of 2D *h*-BN sheet were systematically investigated using DFT. Formation energies of GBs were found to be closely connected with the misorientation angle of GBs. The arrangement of homoelemental bonds on GBs is an important factors which could affect the atomic structures and stability of the *h*-BN sheet. The mechanics of *h*-BN sheets could be significantly affected by GBs. The information obtained in this work would be useful for the understanding of GBs on *h*-BN surface.

### 4. Computational details

The effect of GBs on the mechanical properties of *h*-BN was investigated using DFT, which has been verified as an effective method to calculate the mechanical properties of some other two-dimensional materials (e.g. graphene) as well as those of the GBs on the surface of these materials.<sup>6,21,33-35</sup> Generalized gradient approximation (GGA) with PW91 function<sup>36</sup> was

chosen to describe GBs on *h*-BN surface. The calculation was based on the double-numeric quality with a polarization functions (DNP) basis set. The convergence criterion was given as  $10^{-5}$  a.u. on energy, and  $0.002 \text{ Ha } \text{\AA}^{-1}$  on the maximum force. The self consistent field procedure was carried out with a convergence criterion of  $10^{-6}$  a.u. on energy, and the global orbital cutoff was set as 5.2  $\text{\AA}$ . The periodic boundary condition was performed on the computational unit cell. For all of the GB models, the distance between two GB lines was set to more than 1.5 nm while a vacuum with a height of 1.2 nm was placed above the *h*-BN surface to minimize the influence between adjacent layers and GB lines.<sup>21</sup> A  $6 \times 15 \times 1$  k-point mesh was set up during the geometry equilibrium with all the atomic structure parameters fully relaxed. To obtain the mechanical properties of the *h*-BN with GBs, theoretical stress-strain curves of the systems along the tangential direction and perpendicular to the GBs were plotted by adding a series of uniaxial tensile strain with 1% increment step. Stress was then calculated by the strain energies according to the stress-strain relationship.<sup>6</sup> All calculations were realized using the DMol3 module (Accelrys Inc.).

### Acknowledgements

This work was supported by Centre for Applied Computing and Interactive Media at City University of Hong Kong. It was also supported by a grant from the Shandong Province Special Grant for High-Level Overseas Talents (Grant No. tshw20120745) and the National Natural Science Foundation of China (Grant No. 11404192).

### References

- [1] L. Priester, *Grain boundaries: from theory to engineering*, Springer Press, New York, USA 2012.
- [2] R. Grantab, V. B. Shenoy and R. S. Ruoff, *Science*, 2010, 330, 946-948.
- [3] Y. J. Wei, J. T. Wu, H. Q. Yin, X. H. Shi, R. G. Yang and M. Dresselhaus, *Nature Mater.*, 2012, 11, 759-763.

- [4] M. Y. Gutkin, I. A. Ovid'ko and N. V. Skiba, *Rev. Adv. Mater. Sci.*, 2005, 10, 483-489.
- [5] I. A. Ovid'ko and A. G. Sheinerman, *J. Phys. D: Appl. Phys.*, 2013, 46, 345305.
- [6] J. F. Zhang, J. J. Zhao and J. P. Lu, *ACS Nano*, 2012, 6, 2704-2711.
- [7] Y. I. Jhon, S. E. Zhu, J. H. Ahn and M. S. Jhon, *Carbon*, 2012, 50, 3708-3716.
- [8] T. Zhang, X. Y. Li, S. Kadkhodaei and H. J. Gao, *Nano Lett.*, 2012, 12, 4605-4610.
- [9] K. Kim, Z. Lee, W. Regan, C. Kisielowski, M. F. Crommie and A. Zettl, *ACS Nano*, 2011, 5, 2142-2146.
- [10] C. W. Wang, M. D. Frogley, G. Cinque, L. Q. Liu and A. H. Barber, *Carbon*, 2013, 63, 471-477.
- [11] L. Q. Xu, N. Wei and Y. P. Zheng, *Nanotechnology*, 2013, 24, 505703.
- [12] I. A. Ovid'ko, *Rev. Adv. Mater. Sci.*, 2012, 30, 201-224.
- [13] S. Kurasch, J. Kotakoski, O. Lehtinen, V. Skákalová, J. Smet, C. E. Krill, A. V. Krasheninnikov and U. Kaiser, *Nano Lett.*, 2012, 12, 3168-3173.
- [14] A. Pakdel, C. Y. Zhi, Y. Bando and D. Golberg, *Materialstoday*, 2012, 15, 256-265.
- [15] A. Pakdel, Y. Bando and D. Golberg, *Chem. Soc. Rev.*, 2014, 43, 934-959.
- [16] C. Y. Zhi, Y. Bando, C. C. Tang, H. Kuwahara and D. Golberg, *Adv. Mater.*, 2009, 21, 2889-2893.
- [17] X. B. Wang, C. Y. Zhi, L. Li, H. B. Zeng, C. Li, M. Mitome, D. Golberg and Y. Bando, *Adv. Mater.*, 2011, 23, 4072-4076.
- [18] D. Golberg, Y. Bando, Y. Huang, T. Terao, M. Mitome, C. C. Tang and C. Y. Zhi, *ACS Nano*, 2010, 4, 2979-2993.
- [19] M. Corso, W. Auwärter, M. Muntwiler, A. Tamai, T. Greber and J. Osterwalder, *Science*, 2004, 303, 217-220.
- [20] N. Ding, X. F. Chen, C. M. L. Wu and H. Li, *Phys. Chem. Chem. Phys.*, 2013, 15, 10767-10776.
- [21] Y. Y. Liu, X. L. Zou and B. I. Yakobson, *ACS Nano*, 2012, 6, 7053-7058.
- [22] Z. G. Wang, *J. Nanopart. Res.*, 2012, 14, 756-7.
- [23] A. L. Gibb, N. Alem, J. H. Chen, K. J. Erickson, J. Criston, A. Gautam, M. Linck and A. Zettl, *J. Am. Chem. Soc.* 2013, 135, 6758-6761.
- [24] O. Cretu, Y. C. Lin and K. Suenaga, *Nano Lett.*, 2013, 14, 1064-1068.
- [25] L. C. Gomes, S. S. Alexandre, H. Chacham and R. W. Nunes, *J. Phys. Chem. C*, 2013, 117, 11770-11779.
- [26] S. B. Tang and S. Y. Zhang, *J. Phys. Chem. C*, 2013, 117, 17309-17318.
- [27] X. L. Li, X. J. Wu, X. C. Zeng and J. L. Yang, *ACS nano*, 2012, 6, 4104-4112.

- [28] O. V. Yazyev and S. G. Louie, *Nature Mater.*, 2010, 9, 806-809.
- [29] C. G. Van de Walle and J. Neugebauer, *J. Appl. Phys.*, 2004, 95, 3851-3879.
- [30] J. T. Wu, B. L. Wang, Y. J. Wei, R. G. Yang and M. Dresselhaus, *Mater. Res. Lett.*, 2013, 1, 200-206.
- [31] Y. I. Jhon, P. S. Chung, R. Smith, K. S. Min, G. Y. Yeom and M. S. Jhon, *RSC Adv.* 2013, 3, 9897-9903.
- [32] B. Wang, Y. Puzyrev and S. T. Pantelides, *Carbon* 2011, 49, 3983-3988.
- [33] D. K. Samarakoon, Z. F. Chen, C. Nicolas and X. Q. Wang, *Small*, 2011, 7, 965-969.
- [34] M. Topsakal, S. Cahangirov and S. Ciraci, *Appl. Phys. Lett.*, 2010, 96, 091912.
- [35] N. Ding, X. F. Chen and C. M. L. Wu, *Environmental Science: Nano.*, 2014, 1, 55-63.
- [36] J. P. Perdew and Y. Wang, *Phys. Rev. B*, 1992, 45, 13244-13249.

### Figure captions

Figure 1 Structure of GBs on *h*-BN surface. (a) a GB composed by (5|7) pairs ((2,1)|(1,2)). The repeat vector  $\mathbf{d}$  of GB can be described by the lattice vectors at the left and right domains, respectively. The misorientation angle ( $\theta = \theta_L + \theta_R$ ) is defined to describe the mismatching degree between the two domains; (b) side view of the GB model. The inflection angle was defined to denote the flection degree of the *h*-BN sheet.

Figure 2 Atomic structures of the 15 GBs with their classification based on the symmetry of the GB configurations.

Figure 3 Formation energies of GBs on *h*-BN surface as functions of (a) the inflection angle and (b) the misorientation angle.

Figure 4 Stress-Strain curves of GBs on *h*-BN surface and a pristine *h*-BN along its armchair (BN(AC)) and zigzag (BN(ZZ)) directions. (a) Stress-Strain curves of the pristine *h*-BN and GBs with inflection angle ranges from  $0^\circ$  to  $18.2^\circ$ , (b) from  $24.2^\circ$  to  $28.8^\circ$ , and (c) from  $45.3^\circ$  to  $55.0^\circ$ .

Figure 5 (a) Intrinsic strength of GBs as a function of the inflection angles: hollow triangles for the pristine *h*-BN along armchair and zigzag directions, hollow squares for the GBs. (b) Intrinsic strength of GBs as a function of the misorientation angles: filled circles for the pristine *h*-BN along armchair and zigzag directions, hollow circles for the GBs. The misorientation angle of a pristine *h*-BN surface can be regarded as  $0^\circ$  or  $120^\circ$ .

Figure 6 Distributions of the bond length and the bond angle for the pristine *h*-BN, GB (2,4)|(5,1) and GB (1,5)|(4,3).

Figure 7 Failure processes of (a) an isolated (5|7) pair in GB (4,2)|(3,3)-1; (b) a group of (5|7) pairs in GB (1,5)|(4,3); and (c) a GB line without (5|7) pairs in GB (1,1)|(1,1).

**Table 1** Parameters for the 15 GBs including the structure vector, inflection angle  $\alpha$ , misorientation angle  $\theta$ , the periodic length along GB line  $L$ , formation energy, critical failure strain, intrinsic strength, and classification.

No.	GBs	Inflection angle $\alpha$ [deg]	Misorientation angle $\theta$ [deg]	$L$ [nm]	Formation energy [eV/nm]	Critical failure strain $\delta$ [%]	Intrinsic strength $\tau$ [Gpa]	Class
/	<i>h</i> -BN(ZZ)	0	0	0.252	NA	24 29 <sup>30</sup>	103 102 <sup>30</sup>	/
/	<i>h</i> -BN(AC)	0	120	0.252	NA	18 18 <sup>30</sup>	87 88 <sup>30</sup>	/
1	(1,1) (1,1)	0	60.0	0.432	8.5	17	85	asym
2	(5,0) (5,0)	24.2	121.6	1.403	2.6	14	62	asym
3	(1,0) (0,1)	0	60.0	0.252	7.5	11	78	sym
4	(4,2) (2,4)	38.2	25.7	1.333	5.3	19	54	sym
5	(4,2) (3,3)-1	45.3	10.9	1.310	3.5	17	55	nsym
6	(2,4) (5,0)	55.0	101.5	1.254	5.8	19	34	nsym
7	(4,2) (3,3)-2	50.5	70.9	1.310	8.9	19	42	nsym
8	(2,1) (1,2)	25.5	21.8	0.667	5.1	20	75	sym
9	(1,5) (5,1)-1	34.5	108.7	1.377	4.8	21	51	asym
10	(1,5) (5,2)	38.8	96.6	1.403	7.9	17	47	nsym
11	(4,1) (1,4)	49.5	41.5	1.154	7.7	20	43	sym
12	(2,4) (5,1)	18.2	91.2	1.343	6.2	16	70	nsym
13	(1,5) (5,1)-2	16.8	104.6	1.387	5.5	17	69	asym
14	(1,5) (4,3)	35.6	81.6	1.403	9.1	15	56	nsym
15	(4,2) (4,2)	45.5	85.7	1.333	7.9	20	51	asym

## Table of contents

Grain boundaries have great effects on the mechanical properties and failure behaviors of *h*-BN sheet.

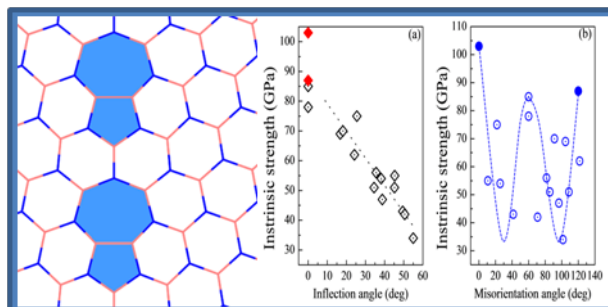


Figure 1

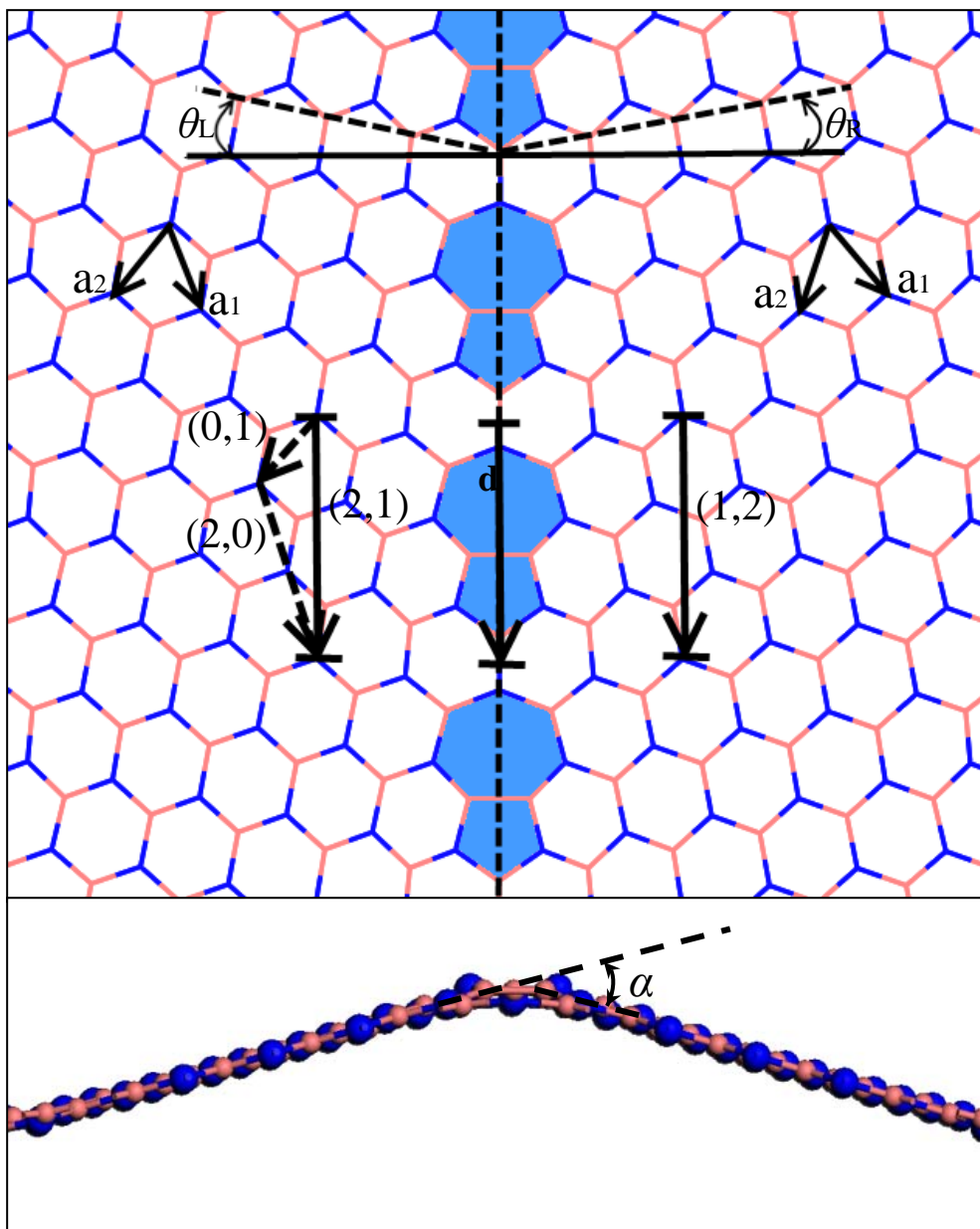


Figure 2

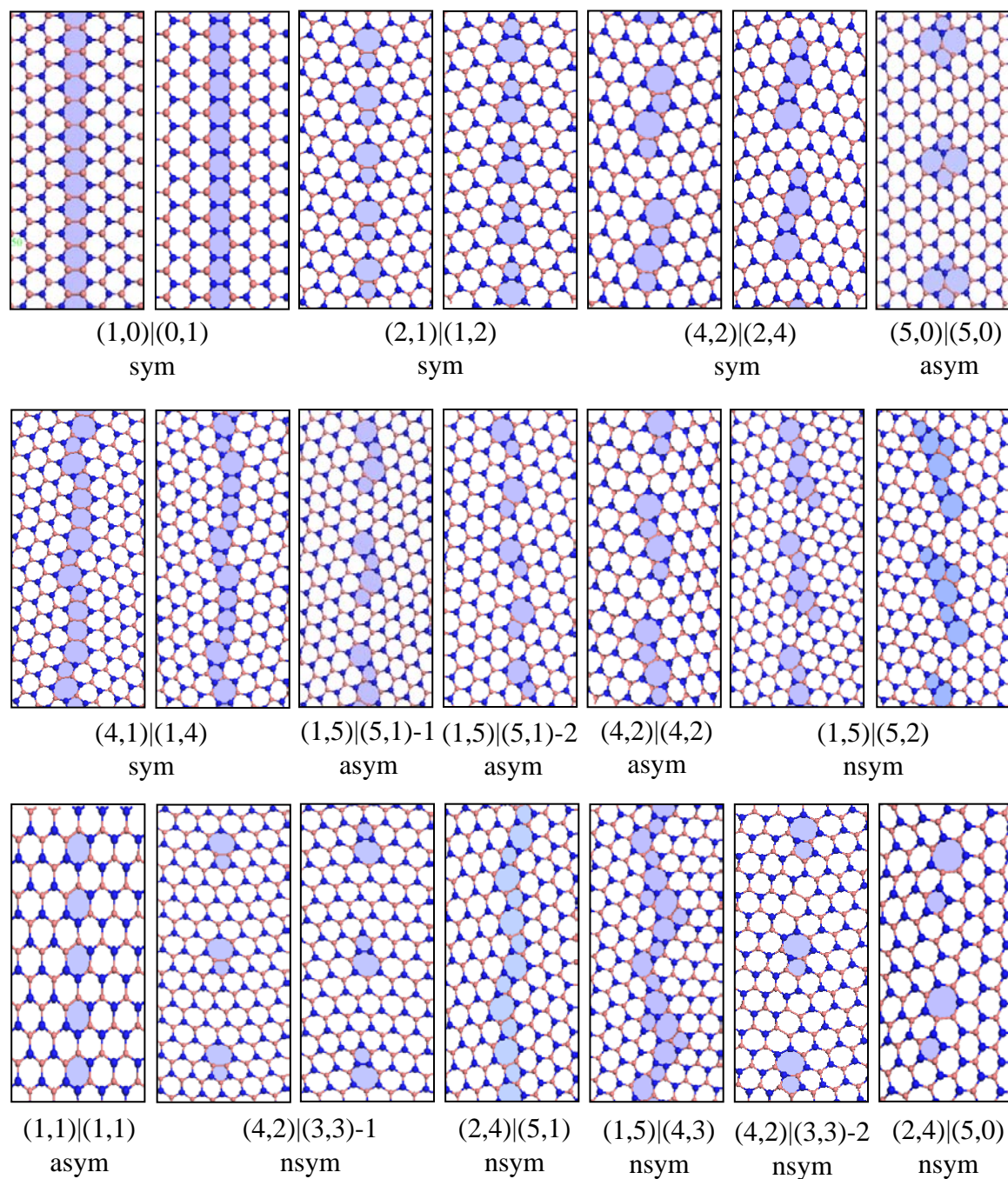


Figure 3

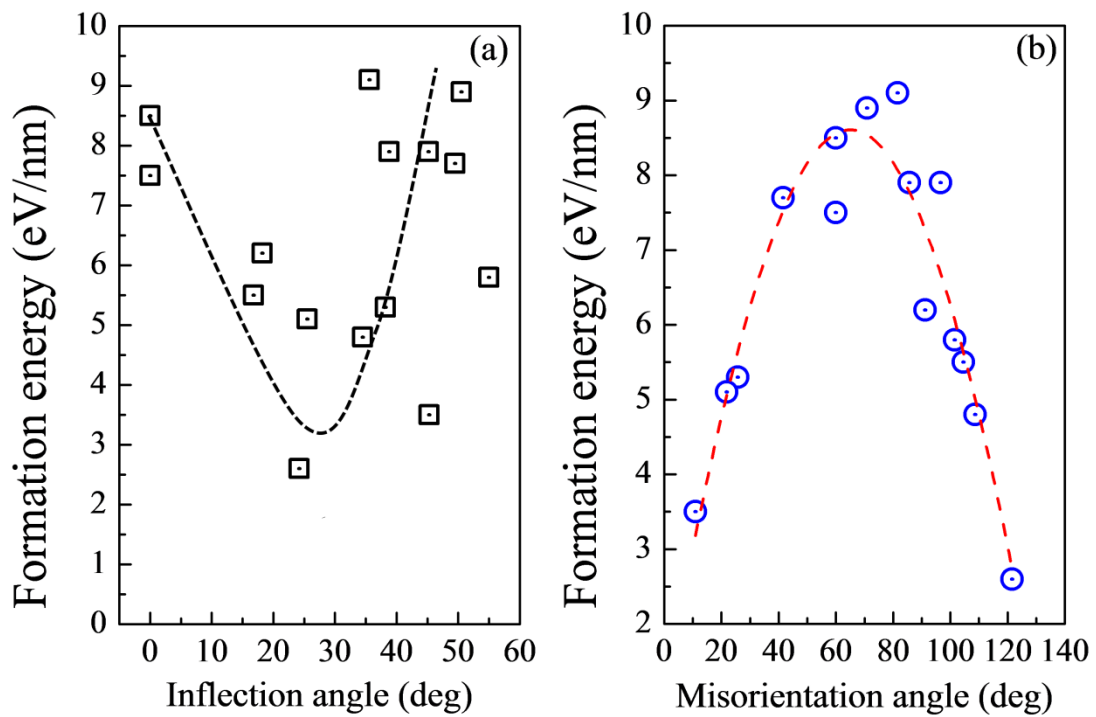


Figure 4

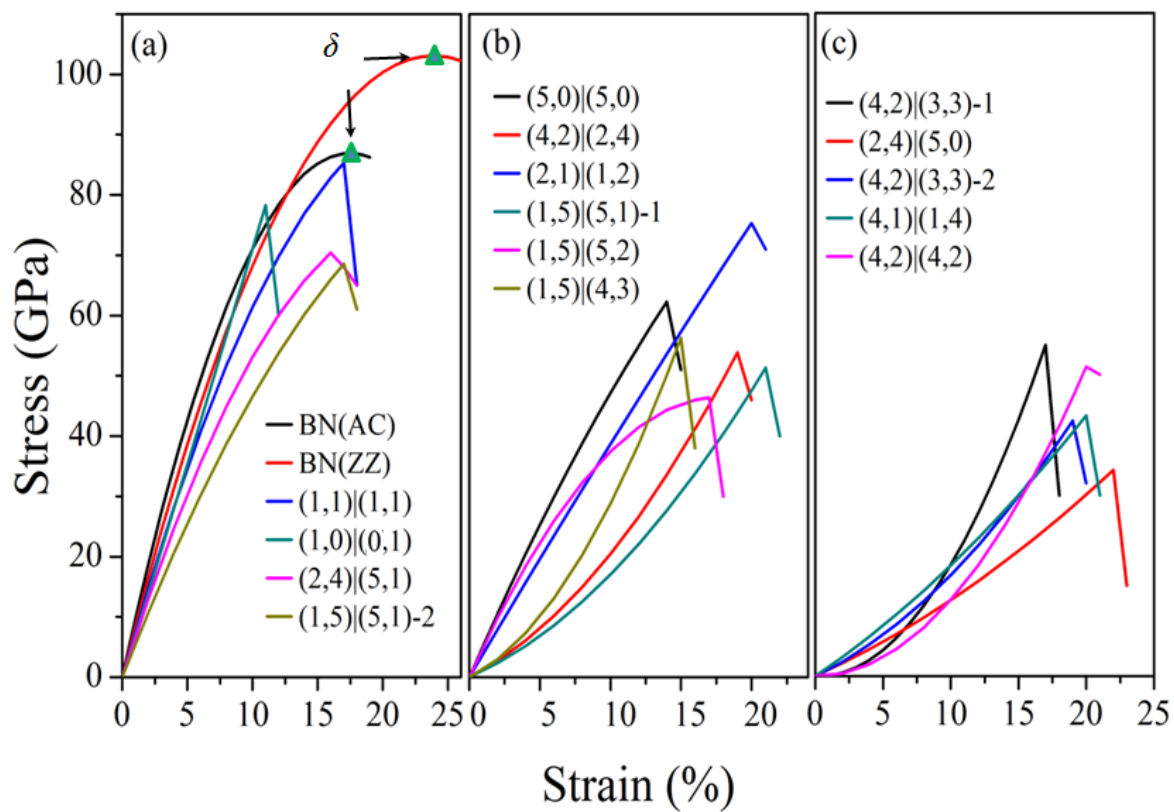


Figure 5

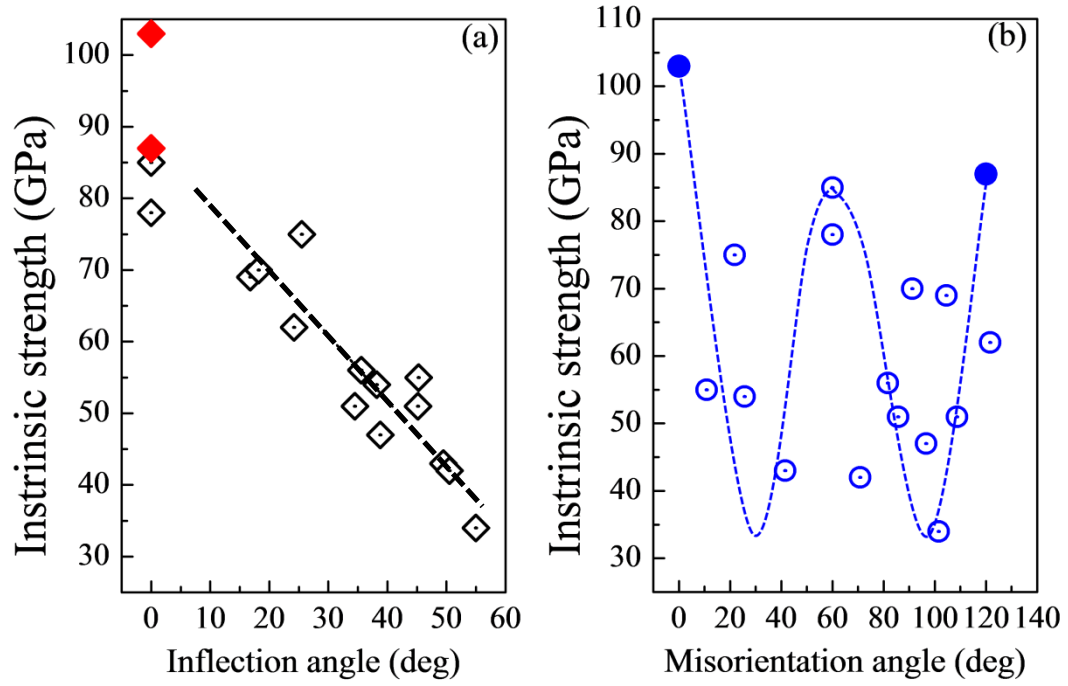


Figure 6

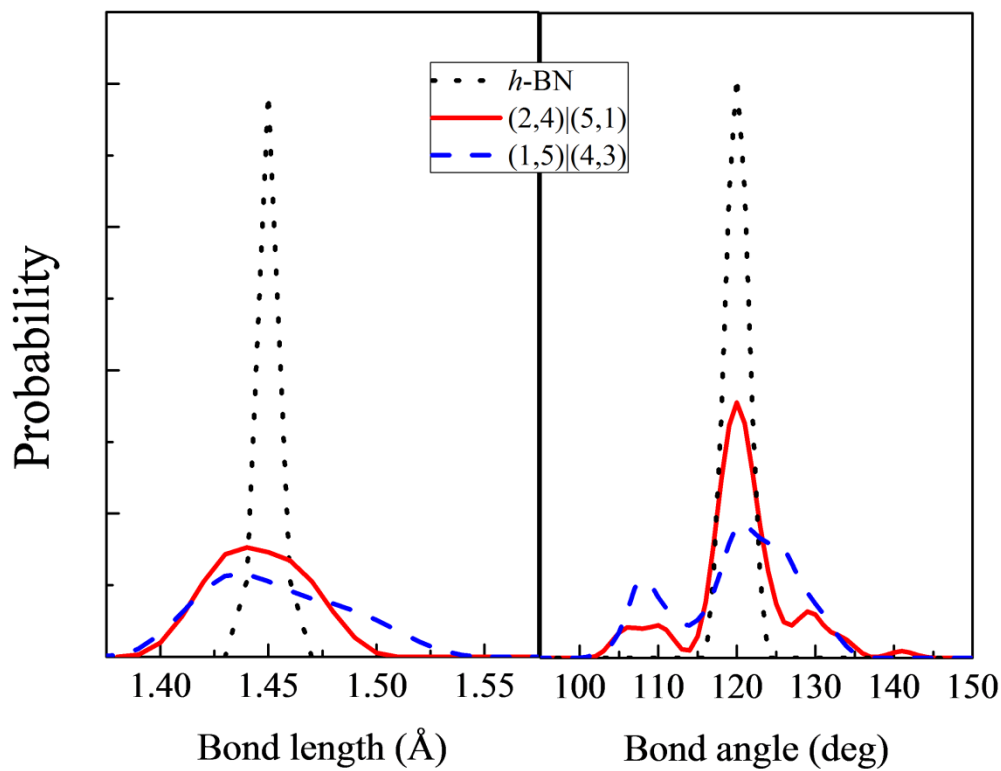


Figure 7

